5684 *Macromolecules* **2009**, *42*, 5684–5699
DOI: 10.1021/ma8000725

Macromolecules
ARTICLE

Gradient Interfaces in SBS and SBS/PS Blends and Their Influence on Morphology Development and Material Properties

Yi Thomann,*,† Ralf Thomann,† Alfred Hasenhindl,† and Rolf Mülhaupt*,†,‡

†*Freiburg Materials Research Center and Institute for Macromolecular Chemistry, Stefan-Meier-Str. 21, 79104 Freiburg, Germany, and* ‡*Freiburg Institute for Advanced Studies (FRIAS), Albertstrasse 19, D-79104 Freiburg, Germany*

Barbara Heck

Polymer Physics, Albert-Ludwigs-Universität, Hermann-Herder-Str. 3, 79104 Freiburg, Germany

Konrad Knoll and Helmut Steininger

BASF SE, Polymer Research, D-67056, Ludwigshafen, Germany

Kay Saalwächter*

Institut für Physik-NMR, Martin-Luther-Universität Halle-Wittenberg, Betty-Heimann-Str. 7, D-06120 Halle, Germany

Received January 11, 2008; Revised Manuscript Received June 14, 2009

ABSTRACT: The formation of gradient interfaces between PS- and PB-rich microphases in SBS block copolymers was investigated by means of solid-state NMR and solution NMR as well as TEM, AFM, and SAXS as a function of molecular architecture, comparing linear and star-shaped asymmetric block structures, and gradient as well as random incorporation of styrene comonomer into the PB-rich blocks. Although all studied SBS possess a very similar total styrene content, different morphologies and mechanical properties were found in the extruded SBS/PS blends, whose origin could be related to the formation of a compositional interface gradient. Employing the sensitivity of solid-state NMR for hard (glassy) and soft (rubbery) phases as well as their respective chemical compositions, we found that upon raising the temperature up to the PS glass transition different amounts of polystyrene from the hard PS phase "soften" and integrate into the soft PB-rich phase ("PS softening"). The degree of "PS softening" characterizes the interfacial gradients of SBS block copolymers at elevated temperatures up to the melt. The softened PS was found to partially mix into the soft phase and partially remain at the interface, thus forming different gradient interfaces, depending primarily on the amount of styrene randomly incorporated in the PB mobile blocks and much less on a compositional gradient at the block linkages in SBS chains. In SBS/PS blends, SBS with a substantial "PS softening" effect was found to preferentially form elongated PB lamellar morphologies, which lead to improved mechanical ductility. The purpose of this study was to apply different characterization methods and correlate their results in order to gain important compositional and morphological information as well as their effects on the SBS/PS blend mechanical properties. Rapid and robust low-cost pulsed solid-state NMR methods were established as versatile analytical tools for application in high-output polymer screening (HOPS) and quality control systems, enabling online monitoring of structure−property correlations as well as product quality of SBS-based materials.

1. Introduction

Poly(styrene-*block*-butadiene-*co*-styrene-*block*-styrene) (SBS) are rubbery/glassy block copolymers, which can be synthesized by means of living anionic polymerization. Since their commercial introduction in the early 1960s,[1] they have been steadily improved. Nowadays, commercially available products can be divided into two basic types: type I "thermoplastic elastomers" with 60−80 wt % soft phase fraction and type II "transparent ductile thermoplastics" with about 20−30 wt % butadiene fraction. All these SBSs can be fine-tuned by varying the sequential comonomer incorporation into the SBS chains or by coupling these chains into star-shaped molecular architectures to achieve specific properties.[2] Kraton introduced by Shell Oil Company, for example, belongs to type I with polybutadiene as mobile blocks, is of rubber kind, and can therefore be used, e.g., as "soft touch" materials. Styroflex from BASF belongs also to type I but with poly(styrene-*co*-butadiene) as mobile blocks. Typical features of Styroflex include optical transparency, high toughness, good adhesion, and processability; its property profile can match that of plasticized PVC but affords better yield strength, elongation, and elastic recovery. Type II SBS has high hard phase fraction and stretch strain and can therefore be used as packaging film, beakers, and other thermoformed as well as injection molded parts. However, most of type II SBSs, especially with styrene incorporated into the mobile blocks, are employed as blend components in general purpose polystyrene (GPPS) in the

*To whom correspondence should be addressed. E-mail: yi.thomann@fmf.uni-freiburg.de (Y.T.); rolf.muelhaupt@makro.uni-freiburg.de (R.M.); kay.saalwaechter@physik.uni-halle.de (K.S.).

 Published on Web 07/15/2009

production of transparent, low-cost impact-modified PS materials.[4] Just this latter type of SBSs and their PS blends will be in the focus of this study.

Previous studies[2,3,5−8] have shown that highly asymmetric SBS multiblock copolymers of both linear and star-shaped molecular architectures can form various complex morphologies, including bicontinuous morphologies, which are generally not found for simple linear diblock copolymers of the same butadiene/styrene composition. However, there are hardly any experimental studies about the interface behavior and its influence on morphologies and especially on morphology formation in melt state as well as its influence on the mechanical properties of the SBS/PS blends. This is probably due to the lack of experimental methods to effectively detect the comonomer contents in both hard PS and soft PB-rich phases. Besides, there are hardly any, or at least no direct, experiments to detect interface gradient behaviors in melt state, where phase morphology is formed, although several SAXS experiments have been described[9] to directly detect interphase thickness in the glass/rubbery block copolymer system. As far as we know, however, these results cannot be adapted to melt systems, where the electron density difference between the phases becomes smaller. Besides, SAXS relies on the assumption of perfect periodical morphology, which is not realizable for most extruded samples. Some measurements using DSC and T_g's as well as microscopic methods to determine the comonomer contents and interface gradient[8,10,11] suffer from limitations in accuracy. Deuterium NMR methods were also used to study the compositional and mobility profile of poly(styrene-*block*-isoprene),[12] but such work can hardly be extended to a wide range of materials, as the method requires specific labeling of segments that are close to the interface. Though in the past decades, interface gradients in block copolymers were often calculated and discussed in terms of thermodynamic theories,[13] experimental methods to detect interface behaviors and their correlations to molecular parameters, morphology formations and material properties in SBS/PS blends still remain highly desirable. As will be shown in this study, by using different proton NMR methods with hard/soft separation focusing on temperature-dependent changes, interface behaviors can be quantitatively investigated and characterized. Besides, we use cost-effective and easy-to-use low-field NMR methods that could ultimately be applied for high output polymer screening (HOPS).[14]

2. Materials and Methods

2.1. Materials. We studied a wide range of SBS copolymers with about the same total comonomer content but various block structures and block linkages, e.g., PB mobile blocks with statistically or gradient copolymerized styrene incorporation, block linkages with an abrupt or gradient composition change, and linear and star-shaped molecular architectures of tri- and multiblock copolymers. Figure 1 illustrates the different types of the investigated SBS, which were synthesized to be analogous to the typical commercially available SBS block copolymers, such as Styrolux (BASF), Finaclear (Total Petrochemicals), and K-Resin (Chevron-Phillips).

The synthesis was done by anionic polymerization in different sequential procedures described in detail in the literature.[2,3] Highly defined linear asymmetrical block, gradient, and random copolymers with long and short PS as end blocks were synthesized. The PS blocks were generally polymerized from styrene without butadiene, whereas the PB-rich mobile blocks and the gradient linkages were polymerized from both butadiene and small parts of styrene. For the star-shaped SBS series a mixture consisting of linear di- or triblock copolymers with short and long PS end blocks was coupled with an oligofunctional coupling agent giving asymmetrical star polymers with an average

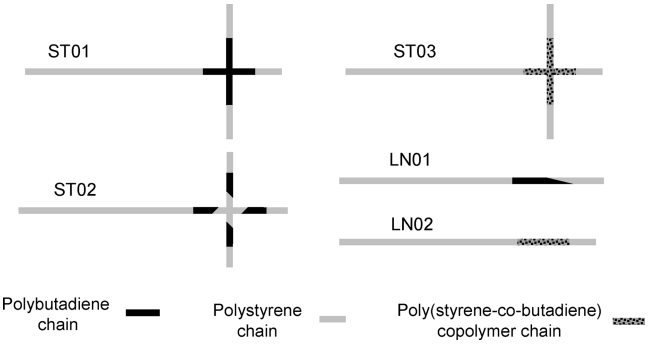

Figure 1. Assumed molecular architectures according to the anionic polymerization procedures and the coupling agents used.

number of four arms,[2,3] one of which with a long and three with a short PS end block. Distributions of short/short and long/long couplings as well as their mixtures are certainly expected, which leads to a molecular weight distribution much broader than that of the original linear block copolymers. All polymers investigated in this study have one feature in common, viz. that they possess about the same total butadiene content. The molecular weight and molecular weight distribution of the investigated SBS's have a range of M_n = 80 000−120 000; M_w/M_n = 1.1−2.3, with linear SBS of 1.1−1.2 and star type SBS of 2.0−2.3, which was determined by gel permeation chromatography (GPC) on polystyrene gel columns from Polymer Laboratories (mixed B type) with monodisperse polystyrene standards at room temperature using tetrahydrofuran as solvent. According to the monomer amounts added in the sequential anionic polymerization procedure and coupling processes, the length ratio of the long and short PS blocks could be calculated to be about 9:1 for star polymers like the sample ST01 and ST03. In case of ST02, the core PS blocks were estimated at about 2.5%−6.5% of the total PS in the block copolymers. The shorter outside PS blocks are somewhat shorter than those in ST01 and ST03, while the longer PS blocks remain about the same. Important composition information on the block copolymers is collected in Table 1, such as the soft phase fractions, the compositions in soft phases, and T_2 values of the soft phases, the temperature dependence of which provides valuable qualitative information on molecular parameters (dynamics, composition), as will be discussed below.

For the blends, a general-purpose polystyrene (GPPS, Polystyrol 158K, BASF) of M_w = 270 000 g/mol and M_w/M_n = 2.6 was used. The components, SBS and GPPS, were compounded for no more than 2 min and extruded at 170 °C into 1 mm thick plates. Such a blending process, excluding oxygen within the extrusion machine, should minimize any oxidation and depolymerization reactions. The final blends appear quite transparent with a slightly milky appearance.

2.2. NMR Experiments and Data Evaluation. ^{1}H solution-state NMR experiments for the determination of the total butadiene content by simple integration of the respective resonances were performed on a Bruker ARX 300 spectrometer operating at 300 MHz using $C_2D_2Cl_4$ as solvent. ^{1}H solid-state MAS spectra served to determine the butadiene content in the soft phase, also by simply integrating the different resonances (Figure 2a−c). MAS experiments were conducted on a Bruker Avance 500 MHz spectrometer operating at 500.2 MHz using a Bruker 4 mm double-resonance probe and a spinning frequency of 4 kHz (with the exception of the data presented in Figure 3, which was obtained on a Bruker Avance II 400 MHz with similar setup). The sample temperatures were 299, 309, 336, 363, and 392 K. Under these conditions, all individual resonances of the soft phase are well resolved, while the hard part is not yet broken up into spinning sidebands and thus forms a broad contribution to the baseline (Figure 2a). After subtracting the contribution belonging to the PS hard phase (simply by

Table 1. Characteristics of the Investigated SBS Block Copolymers

		ST01	ST02	ST03	LN01	LN02
total PB content[a] $x_{PB,total}$	H%	31.7	30.3	31.1	31.8	30.2
	wt %	23.4	22.9	24.0	24.3	23.0
	mol %	36.6	37.6	38.3	36.7	38.2
1,2-PB units in PB[a]	%	12.0	8.4	12.9	11.3	12.3
T_2 at 299 K[b]	μs	655	666	525	590	465
soft phase fraction[b] at 299 K f_s	H %	30.0	30.8	33.8	35.2	29.6
	wt %	22.4	23.8	26.8	28.1	22.4
	vol %[e]	25.5	26.9	30.3	31.7	25.5
PB content in soft phase at 299 K (indirect)[c]	H%	105.7	98.2	92.0	90.5	102.0
	wt %	108.5	97.5	88.8	86.8	102.9
	mol %	104.2	98.7	93.9	92.6	101.5
PB content in soft phase at 299 K (direct)[d]	H%	96.6	92.8	85.1	77.1	84.1
	wt %	95.1	89.9	79.8	70.0	78.6
	mol %	97.4	94.5	88.4	81.8	87.6
soft phase fraction[b] at 309 K f_s	H%	32.0	32.4	36.7	36.7	32.8
	wt %	24.7	25.4	30.0	29.8	26.0
	vol %[e]	28.0	28.8	33.7	33.5	29.4
PB content in soft phase at 309 K (indirect)[c]	H%	99.1	93.6	84.7	86.6	91.9
	wt %	98.7	91.0	79.4	81.8	88.8
	mol %	99.3	95.1	88.1	89.6	93.8
PB content in soft phase at 309 K (direct)[d]	H%	95.8	92.0	80.8	76.8	80.6
	wt %	94.0	88.9	74.5	69.6	74.2
	mol %	96.8	93.9	84.9	81.5	84.7
soft phase fraction[b] at 336 K f_s	H%	37.6	36.8	44.1	42.8	42.8
	wt %	30.8	30.3	38.2	36.6	37.0
	vol %[e]	34.6	34.0	42.3	40.6	41.0
PB content in soft phase at 336 K (indirect)[c]	H%	84.4	82.4	70.5	74.3	70.5
	wt %	78.9	76.4	62.3	66.8	62.3
	mol %	87.8	86.2	76.1	79.5	76.1
PB content in soft phase at 336 K (direct)[d]	H%	92.5	89.2	74.6	75.3	71.3
	wt %	89.5	85.1	67.1	67.5	63.3
	mol %	94.3	91.7	79.7	80.0	76.8
soft phase fraction[b] at 363 K f_s	H%	43.3	43.0	52.1	48.8	51.5
	wt %	37.2	37.2	47.1	43.3	46.6
	vol %[e]	41.3	41.2	51.3	47.5	50.8
PB content in soft phase at 363 K (indirect)[c]	H%	73.1	70.4	59.7	65.1	58.6
	wt %	65.4	62.2	50.6	56.4	49.5
	mol %	78.4	76.0	66.4	71.4	65.4

[a] Determined by solution-state ^{1}H NMR in $C_2D_2Cl_4$ (aromatic and olefinic signals). [b] Determined by low-field solid-state ^{1}H time-domain NMR. [c] Determined *indirectly* from the total butadiene content from solution NMR and the soft phase fraction from low-field NMR, with the preliminary assumption that all PB is mobilized in soft phase. [d] Determined *directly* by high field solid-state ^{1}H MAS NMR (integration of aromatic and olefinic signals). [e] Volume fractions are calculated on the basis of the bulk densities $\rho_{PS,299\,K} = 1.04$ g/cm^3; $\rho_{PS,364\,K} = 1.02$ g/cm^3; $\rho_{PS,299\,K} = 1.07$ g/cm^3; $\rho_{PS,364\,K} = 1.02$ g/cm^3 (the latter two are extrapolated from the melt); $\rho_{PB,299\,K} = 0.88$ g/cm^3; and $\rho_{PB,364\,K} = 0.85$ g/cm^3 and the respective molar masses, taking into account the soft-phase composition obtained by ^{1}H MAS NMR and assuming a linear mixing law for its density. All densities are extracted from the PVT data conducted on a Gnomix PVT apparatus.

applying a baseline correction), spectra showing only the contributions from the soft phase can be obtained. (Figure 2b,c). Along with the signal assignments, the chemical composition in the soft phase can be inspected, for which the integral of the respective resonance peaks is evaluated (Figure 2c).

For the investigation of the compositional interface gradient, a special DQ-filtered MAS spin diffusion pulse sequence was applied, which is identical to a conventional DQ build-up experiment with a very short DQ evolution time (selecting the hard, strongly dipolar-coupled phase) and a variable *z*-filter. In this experiment, the selected hard-phase magnetization is subject to a spin diffusion process between fixed spins during the *z*-filter, mediated by energy-conserving dipolar flip-flop processes, into the mobile phase. The rising, well-resolved signals of the PB and PS components as a function of spin diffusion time carry quantitative spatially resolved information on the interphase composition. Details on this ^{1}H MAS spin diffusion experiment have already been published as a separate paper.[33]

A 0.5 T Bruker Minispec mq20 low-resolution NMR spectrometer (19.9 MHz proton Larmor frequency) was used for the determination of the soft phase fraction, for spin diffusion experiments for domain size estimation,[15] and for the determination of T_2 relaxation times for the soft phase. Phase specificity is straightforwardly realized by decomposition of the free induction decay (FID) signal, as detailed on the example of the K-Resin sample in ref 21. The samples in the form of granules were always restricted to the bottom 5 mm of 10 mm o.d. sample tubes and placed in the center of the coil for good rf homogeneity. The Minispec provides 90° pulses of less than 2 μs length and a fast digitizer; yet the dead time of about 12 μs precludes a precise quantification of solid components, the FID signal of which is typically dephased within 30 μs by the multiple strong dipolar couplings (while the couplings in the soft phase are almost fully averaged due to mobility). This problem is commonly solved with the help of a solid echo, where many experiments with variable echo delays and an extrapolation have to be performed because a solid echo cannot fully refocus multiple dipolar couplings in a dense proton system. See ref 16 for recent applications of this approach. We employ the pulsed version of the mixed magic-sandwich echo (MSE),[17] which forms a full multispin dipolar and chemical-shift echo after a total delay of 76 μs and thus removes the necessity for solid-echo time extrapolation. This is described in detail in ref 18, where we show that its implementation on the Minispec serves to almost quantitatively refocus the ^{1}H magnetization and thus allows the detection of almost the complete sample magnetization as the intensity at the echo top—the signal loss associated with the rigid-phase amounts to only about 10%.[18,21] Figure 2d shows the MSE-refocused FID's, taken at three different temperatures on the example of ST02, where time = 0 corresponds to the echo

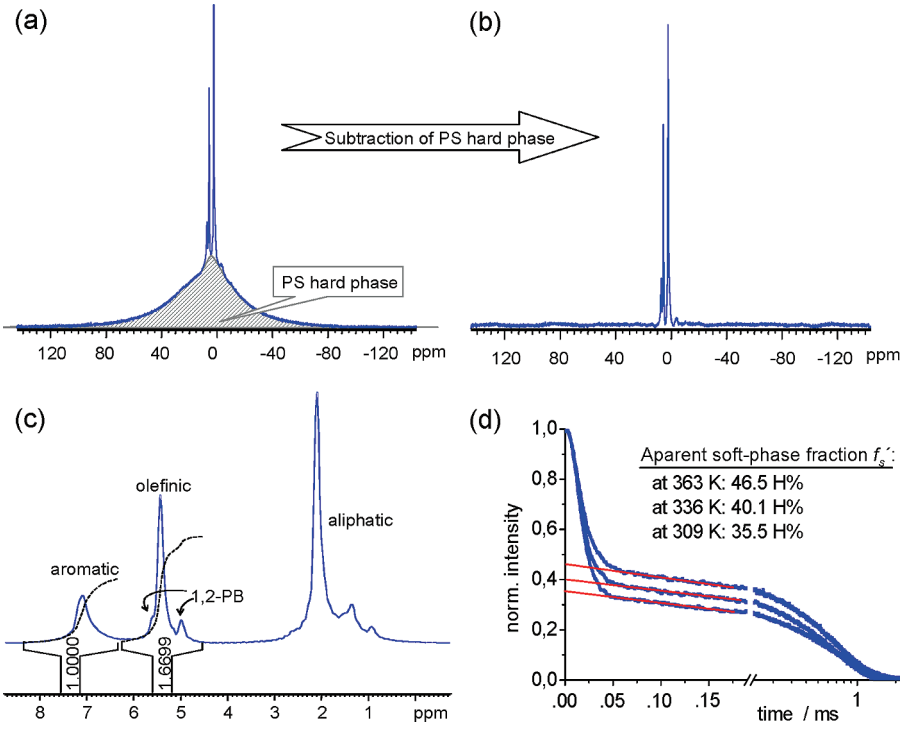

Figure 2. (a) ^{1}H solid-state NMR spectrum of the ST03/GPPS 40/60 blend spun at 4 kHz at $T = 299$ K. (b) The same spectrum after subtracting the PS hard phase halo, using the baseline correction tool of 1D WinNMR V6.2 from Bruker. (c) ^{1}H solid-state NMR spectrum along with the signal assignments and integral proportions of ST03 spun at 4 kHz at $T = 336$ K. (d) MSE-refocused ^{1}H FID of ST02 at different temperature, recorded on the low-field Minispec. The lines are linear fits of the data between 0.06 and 0.16 ms and is used for the back-extrapolation of the soft phase fraction in H%.

maximum. It can be seen that the signal shape of the individual components hardly changes, allowing for an accurate decomposition at all temperatures. A linear back-extrapolation of the FID region between 0.06 and 0.16 ms provides a sufficiently accurate estimate for the soft phase fraction (obtained in units of proton number), which increases with increasing temperature. This is discussed in detail in ref 21. Here, we just note that the soft phase is reliably described by a simple, slightly stretched exponential contribution, while the rigid phase consists of a Gaussian part, and a slightly mobilized interphase contribution with stretched exponential shape, but with an overall short decay time similar to the Gaussian part (~25 μs). This interphase is thus treated as part of the rigid fraction, rendering all the materials in this study effectively two-phase from the dynamic point of view. As shown in ref 21, the systematic error inflicted on the rigid fraction by the simple linear extrapolation rather than full component fitting is another 5%, such that we up-correct the extrapolated rigid fractions $f'_{r,H\%} = 1 - f'_{s,H\%}$ by 1.15 and obtain $f_{s,H\%} = (f'_{s,H\%}/(f'_{s,H\%} + 1.15f'_{r,H\%})) \times 100 = (40.1/(40.1 + 1.15 \cdot 59.9)) \times 100 = 36.8$ H% for sample ST02 at 336 K.

Determination of Phase Composition. It is one major purpose of this paper to demonstrate that simple low-field data analyzed in an easily automatable fashion (Figure 2d), combined with the *overall* composition information that is readily obtained from solution-state NMR, can be used for a composition estimation of the individual phases, which is accurate enough to establish structure−property relations, as shown in the later sections. This obviates the need for dedicated high-resolution MAS solid-state NMR equipment. We therefore give the details that are important to support our claim. We note at the outset that the low-field procedure for soft- and hard-phase quantification is more accurate than the integration of the slow-MAS spectra (see Figure 2a), which suffers from baseline problems (e.g., due to probe background) and phase correction issues, thus giving an overestimated hard-phase (underestimated soft-phase) content.

For completeness, and to highlight all conversions involved in the data given in Table 1, we first exemplify the conversion of the soft phase fractions f_s in H% (Figure 2d) into wt %, which is based on the preliminary assumption that all PB is mobilized in the soft phase:

$$f_{s,wt\%} = ((54.08x_{PB,total,H\%}/6)+104.04(f_{s,H\%} - x_{PB,total,H\%})/8)/ ((54.08x_{PB,total,H\%}/6)+104.04(100 - x_{PB,total,H\%})/8) \times 100$$

where $x_{PB,total,H\%}$ is the total PB content of the SBS in H%, $f_{s,H\%}$ is the soft phase fraction in H%, 104.04 is the molecular weight of styrene, 54.08 is the molecular weight of butadiene, 8 is the number of protons on styrene, and 6 is the number of protons on butadiene. The calculation of the vol % of the soft phase is a bit more involved, and details are outlined in the corresponding footnote to Table 1.

Using the quantitative soft phase fraction and the additional information on the overall PB content from solution ^{1}H NMR (see Table 1), the *indirect* yet cost-efficient and high-output compatible method to estimate the soft-phase composition of the samples is also simply based on the assumption that all PB is mobilized in soft phase at all temperatures. This is in fact true in the higher temperature range above 336 K, where no PB is found to be included in hard phase of our samples (see below). Taking LN01 at 336 K as an example, the PB content in the soft phase $x_{PB,soft,indirect}$ is easily obtained as follows:

$$x_{PB,soft,indirect} = (x_{PB,total,H\%}/f_{s,H\%}) \times 100 = (31.8/42.8) \times 100 = 74.3H\%$$

From the results in H%, the mol % and wt % are straightforwardly determined, considering molecular weights and the proton numbers of the repeat units. The sample result thus suggests that the soft phase contains around 25 H% of *mobilized* PS.

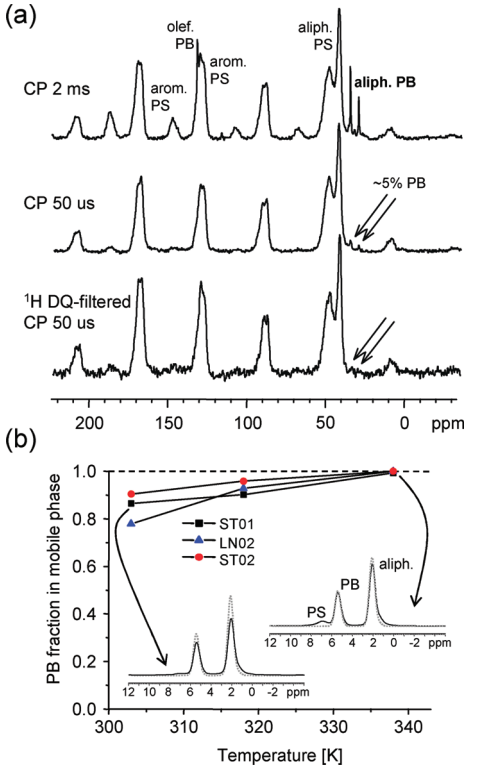

Figure 3. Quantitative investigation of PB partitioning. (a) ^{13}C CP MAS NMR spectra of ST01 spun at 4 kHz at $T = 300$ K: the upper two spectra differ in the contact time, and the bottom spectrum was obtained with an additional rigid-phase selective ^{1}H double-quantum filter before CP. (b) PB fraction in the mobile phase (relative to the overall PB content) determined by quantitative ^{1}H MAS NMR at 4 kHz spinning. The insets show spectra of ST01 (solid lines) in comparison to PB homopolymer spectra (dashed lines) scaled to the expected intensity based on sample weights. For these plots, 300 Hz Gaussian line broadening was applied to render the signal shapes comparable; integrations were performed on unapodized spectra.

The *direct* yet of course experimentally more involved method is to evaluate the integrals in the MAS spectra, as shown exemplarily in Figure 2c, where for LN01 at 336 K we obtain $x_{PB,soft,direct} = 75.3$ H%. It is in principle expected that the indirect method underestimates the PB content at 336 K and higher, but overestimates at lower temperature and in cases where there is substantial PB immobilized in the hard phase. The latter leads even to values above 100% for some samples (see Table 1). The latter is even more clearly apparent from Figure 11a, which will be discussed in section 3.2.3, where, with more data points, direct and indirect $x_{PB,soft}$ at 299 K are shown in the same diagram for comparison.

Finally, we need to evaluate the quality of the crucial assumption that most PB is mobilized in the soft phase. For this purpose, we performed auxiliary ^{13}C CP MAS and quantitative ^{1}H MAS experiments, as summarized in Figure 3. At longer contact times (2 ms), the ^{13}C spectra in Figure 3a exhibit contributions from both phases, while at 50 μs CP, the spectra are at least dominated by rigid-phase signal. Since there is considerable overlap in the aromatic and olefinic regions, PS and PB can be separated only in the aliphatic region, where from the short-CP spectrum, a 5% PB content of the hard phase can be roughly estimated. Appending a short ^{1}H DQ filter (in analogy to the DQ-filtered spin diffusion work published in ref 33 and discussed below), further suppression of the residual PB signal is achieved (indicating a lower amount), yet at the expense of more noise and impracticably long experimental times (as the DQ filter retains only 25% of the ^{1}H signal). In all, the ^{13}C data demonstrate that the hard phase of ST01 at 300 K indeed contains a small amount of PB, but truly quantitative data cannot be obtained within reasonable times.

The PB−PS quantification is in fact more easily possible with ^{1}H MAS spectra (see Figure 2c), and we thus performed quantitative investigations by using samples with calibrated weight, confined to the center of the rotors with spacers, and measuring at identical receiver gain. As an intensity reference, we measured pure linear PB of similar microstructure (vinyl content) and could thus quantify how much PB is "missing" in the ^{1}H MAS spectra of the SBS samples. The results shown in Figure 3b clearly show that there is no missing PS above 336 K, which confirms the viability of the indirect method. Note that such a quantification, while being more time-consuming, could in principle be performed on the basis of ^{13}C Bloch decay spectra with a short recycle delay, relying on the shorter mobile-phase ^{13}C T_1 (~0.5 s for aliphatic PB). However, transient NOE effects related to the necessary ^{1}H decoupling require recycle delays in excess of 7 s ($5 \times T_1^{1H}$) for truly quantitative spectra, after which the hard-phase signals already contribute significantly, rendering the acquisition of pure soft-phase ^{13}C spectra difficult ($T_1^{PSrig} \approx 30$ s, not unlikely less for immobilized PB). This once more highlights the potential pitfalls related to ^{13}C spectroscopy.

Spin Diffusion for Domain Size Estimation. Spin diffusion measurements with the Minispec were performed using the traditional Goldman−Shen pulse sequence[19] before the mixing time t_{mix}, but also with the MSE before the final detection. In this way, it is possible to determine the magnetization distribution among the phases at any time during the spin diffusion process, which is a decisive advantage over the often used approach for proton-detected spin diffusion,[20] where only the mobile signal is evaluated and has to be corrected for T_1 relaxation effects. In our approach, the T_1 effect can directly be followed in terms of the decay of the overall magnetization. Here, we apply a simple first-order correction by analyzing a normalized $I(\text{soft})/I_0(\text{total})$. The effect of T_1 is generally complex, as diffusing and relaxation occurs simultaneously, leading to nonexponential relaxation behavior and complex spin diffusion curves in each of the phases. These aspects are treated in detail in a separate publication.[21] For the present case, we noted that our procedure provides good estimates when only the initial decay is analyzed in the usual way, i.e., by linear fitting in a plot vs sqrt(t). Sample data are shown in Figure 4a. As the mobility contrast between the phases was always as well-defined as seen in Figures 2d and 4a (no large detectable phase with intermediate mobility), there was no necessity to employ a more elaborate dipolar-filter sequence.[22]

Figure 4b shows an example of a plot of I/I_0 vs $t_{mix}^{0.5}$. Notably, the data do not level out at the intensity plateau that is typically observed in high-field experiments.[20] This is a consequence of the signal loss due to the very short T_1 at low field, which is of the order of a few hundred milliseconds. The initial linear decay can however be fitted with good accuracy, from which the characteristic spin diffusion time $t_0 = 257$ ms is determined and evaluated under the assumption of a lamellar geometry:[15]

$$d_{soft} = (2\varepsilon/\sqrt{\pi})[D_{eff}t_0]^{1/2} \quad (1)$$

Here, ε is the number of orthogonal directions relevant for the spin diffusion process. Its value depends on the morphology and is 1 for lamellar block copolymers, 2 for phases with a cylinder-like morphology in a matrix, and 3 for discrete phases (e.g., spheres) in a matrix.[15] The assumption of lamellar morphology in our case is based on the TEM investigations, although the lamellar morphologies are not very ordered. The effective spin diffusion coefficient D_{eff} is calculated as

$$\sqrt{D_{eff}} = \frac{2\sqrt{D_{soft}D_{hard}}}{\sqrt{D_{soft}}+\sqrt{D_{hard}}} \quad (2)$$

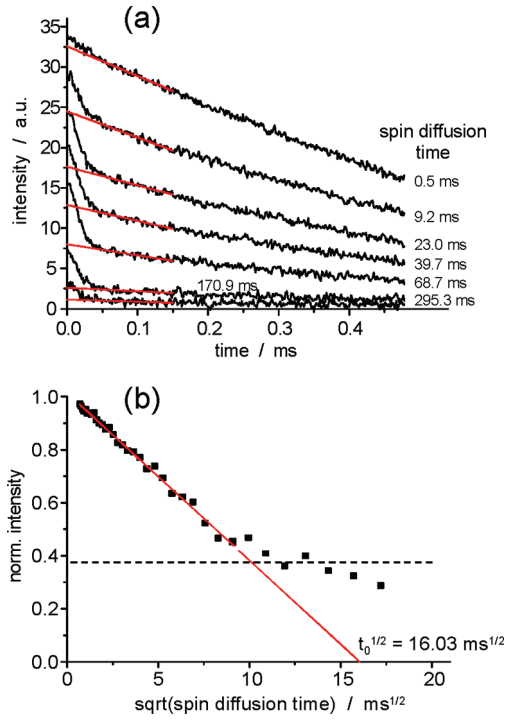

Figure 4. (a) Sequence of MSE-detected FIDs in a series of ^{1}H spin diffusion experiments with increasing mixing time and (b) relative soft-phase magnetization I/I_0 curve for ST01 at $T = 336$ K. The solid line in (b) is a linear fit to the initial decay to determine the characteristic spin diffusion time ($16.03^{0.5}$ ms$^{0.5}$)^2 = 257 ms, from which the domain thickness can be calculated by aid of eq 1. The dashed line indicates the soft phase fraction of the sample, and the fact that the data does not level out at this plateau indicates the shortcomings of the simplified T_1 correction.

where the spin diffusion coefficient of PS hard phase D_{hard} is known to be 0.8 nm^2/ms[15] and the coefficient for the soft phase D_{soft} is calculated following the calibration of Mellinger et al.[20] from its apparent T_2 relaxation time that was also measured on the Minispec using a simple incremented Hahn echo. For details, we also refer to ref 21. In all samples over the investigated temperature range, the transverse relaxation decays were nearly monoexponential and fitted accordingly.

2.3. Small-Angle X-ray Scattering (SAXS). The SAXS measurements were performed in an evacuated Kratky compact camera (Anton Paar K.G., Graz, Austria) with an 80 μm entrance slit. Cu Kα radiation with a wavelength of $\lambda = 0.154$ nm was used. The scattered intensity I was recorded by a scintillation counter in a step-scanning mode at room temperature. A beam stopper was used to prevent the primary beam entering into the detector at lower angles. The scattering profiles were corrected for background scattering and desmeared using Strobl's algorithm.[23] The measurements were performed in an s range of 0.012−0.8 nm^{-1}.

2.4. TEM/AFM Imaging. Morphological details of the samples were examined by using a transmission electron microscope (LEO 912 Omega, ZEISS) applying an acceleration voltage of 120 kV as well as by using atomic force microscopy (MultiMode AFM with Nanoscope IIIa controller, Digital Instruments). For TEM, the butadiene phases were selectively stained with osmium tetroxide (OsO_4) prior to microtoming. Generally, the sample preparation could be done in one step: the ultrathin sections were gathered for TEM, and the surface of the remaining bulk material was used for AFM investigations. In this study we used a Leica Ultramicrotome; ultrathin sections were prepared for TEM investigations. AFM was done on a MultiMode AFM apparatus of Veeco Instruments Inc. with the Tapping Mode technique. Height and phase images were simultaneously taken. The picture contrast in phase images are generally responsible to hard/soft material contrast. In both AFM phase images and TEM micrographs, PS hard phase appears brighter and soft polybutadiene-rich phase appears darker. Methods and comparisons of TEM and AFM micrographs in heterogeneous polymer systems were described in detail in previous publications.[24,25]

2.5. Mechanical Property Measurements. The SBS/PS blends were tested with a tensile testing machine (Z005, Zwick GmbH & Co.). The 1 mm thick film was cut along and perpendicular to the extrusion direction. The tensile length was about 50 mm. Young's modulus, stress, and strain at break were evaluated from the stress−strain curves. At least five test samples were tested for each blend film to get statistically valid test results. Only the strain at break ε_B will be discussed in the results. ε_B is also occasionally called tensile ductility, which expresses its relation to molecular mobility.

3. Results and Discussion

By using NMR, SAXS, and TEM/AFM, the SBS's were systematically studied and their morphology development in SBS/PS blends were investigated in detail. Actually, all these methods are able to give morphology information from different viewpoints. The microscopic methods TEM and AFM give a direct visualization of the phase structure with a resolution down to the nanometer scale and within a rather localized area. Spectroscopic and scattering methods, like NMR and SAXS, give averaged information over much larger scales of the samples. Moreover, NMR offers insights into the chemical composition within the (hard and soft) phases and the phase boundaries, and SAXS provides long-range periodicity of domains with different electron density. In this study, we compare and correlate the results from all these techniques, giving us a broad understanding of the morphological development and its influence on the material properties.

3.1. Small-Angle X-ray Scattering (SAXS) in SBS and SBS/PS Blends. To detect the long period both in SBS and in SBS/PS blends, SAXS experiments were done. We first intended to test the effect of PS blending into SBS and expected an increase in the averaged long period in the blends in comparison to the mere SBS's. Yet this was not the case, as corroborated by both the SAXS results shown here or by TEM shown further below. Figure 5 shows the SAXS diagrams of the SBS block copolymers and their 40/60 SBS/GPPS blends. Most long periods in blends remain the same as in their block copolymers. In some blends, the long periods became even somewhat smaller, which is in contradiction to the expectation. This indicates that most SBS lamellae retain their spatial correlation in the blends. As is well-known, SAXS detects the most frequently appearing periodic structure, i.e., the accumulated SBS part in the blends, not the diffuse and detached SBS part. As for the slightly decreased long period in some blends, it could be the result of enhanced ordering of the block copolymer morphology after the PS is blended into the SBS's and is also reflected in the increased intensity of the SAXS peaks. The intensity in the diagrams is normalized with respect to the sample thickness. Therefore, if the degree of ordering before and after blending would remain the same, the intensities in the blends should be about 60% as compared to pure SBS's. Apart from the peak intensity, the integral of the SAXS curves can also give an estimate as to the PS incorporation within the soft phase SBS's because of the reduced electron density difference between the two phases. For example, LN02 has a much lower signal intensity than other block copolymers, which is due to the strong PS incorporation into the PB-rich mobile blocks and reduced scattering contrast

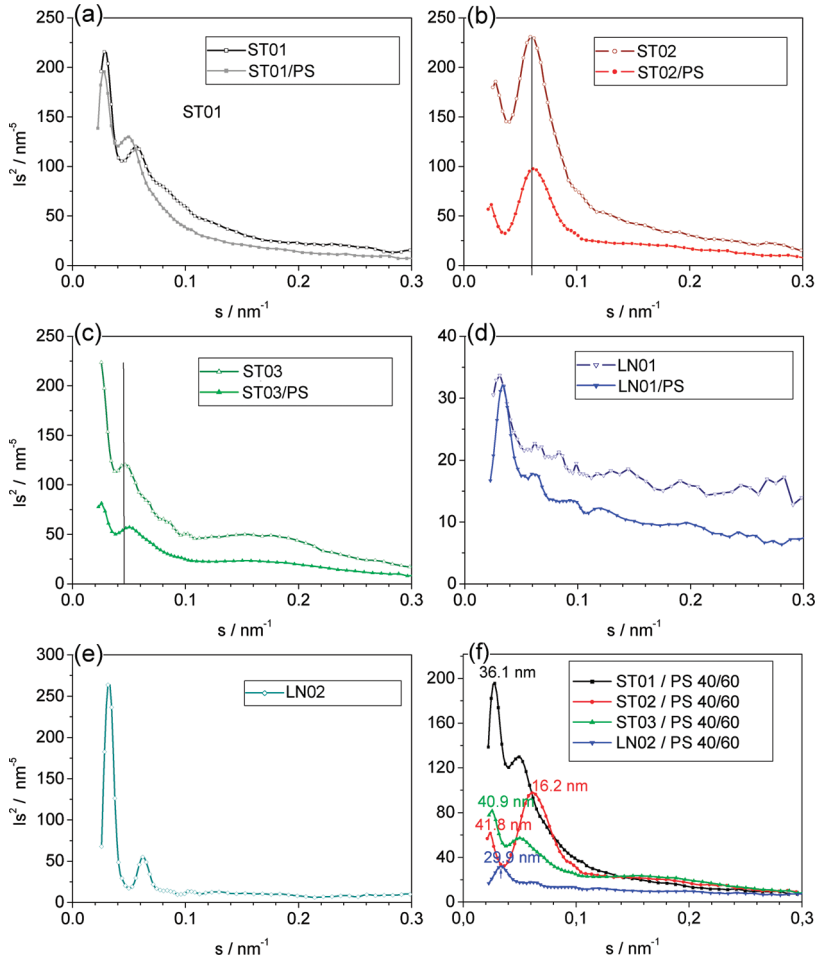

Figure 5. SAXS diagrams of the SBS's and 40/60 SBS/GPPS blends: the long periods were evaluated from the first-order peaks. Because of the low degree of ordering and the mixed morphologies, the peaks of higher order of most samples could not be evaluated. The peaks for the double lamellae are not of higher orders.

between the phases. This is in accordance with the NMR results shown below. Therefore, in our SBS system, the SAXS intensity could be influenced by the ordering grade as well as by PS content in the soft phase.

Another noticeable point of the SAXS study is that in the diagram of ST02/GPPS the second peak is more intense, which could be assigned to double lamellae. The double lamellar morphology in this sample could also be directly seen in the TEM micrograms shown below (see Figure 14e,f). Again, the strong peak of the double layers is the result of the most frequently appearing periodicity. Interestingly, the signal intensity of this peak is about 60% in the 40/60 blend in comparison to its block copolymer, which means that blending with PS has no effect on the double layer. Also, the scattering angle remains the same in blends as in pure SBS, meaning that there is no PS mixed into the double lamellae upon the PS blending.

For the evaluation of the individual phase dimensions, a very ordered morphology is needed. Because of irregularities and complex periodic morphologies (e.g., lamellae mixed with gyroid-type structure) according to the SAXS diagrams, we refrain from a quantitative discussion of individual lamellar thicknesses. However, the long period values read off from the SAXS diagrams were of use when combined with the soft phase fraction determined by low-field NMR measurements for comparisons of domain sizes, as discussed below.

Also, an interphase width evaluation from the SAXS diagrams, as described by Hashimoto et al.,[9] is based upon a perfect periodicity, which could only be obtained by carefully evaporating procedures from solution. Moreover, certain models must be used for the interphase width evaluation with SAXS. The fact that most SBS's or SBS/PS do not form perfectly lamellar or other periodic morphologies, especially under extrusion conditions, prevented us from using this method to evaluate the possible interphase width.

3.2. NMR. High-resolution solution ^{1}H NMR was used to determine only the total comonomer content in the SBS's, and high-field solid-state ^{1}H MAS NMR was used to determine the comonomer contents in the soft phase. With low-field solid-state NMR it is possible to separate soft from hard components and thus to determine the phase composition directly and precisely from chemical shifts in the spectra. If needed, an additional temperature variation is also possible. These are the major advantages as compared to the composition analysis by T_g shifts from DSC measurements, while the latter is of course quite easy to do and first choice for a quick analysis.[10] Moreover, we used an industrial low-field NMR instrument (the Bruker Minispec) to obtain a variety of useful characteristics. Apart from the missing chemical-shift resolution, this approach shares the versatility and accuracy of high-field pulsed solid-state NMR (where the sensitivity difference is partially offset by the use of higher sample amounts) and is as easy to use and cost-effective as DSC.

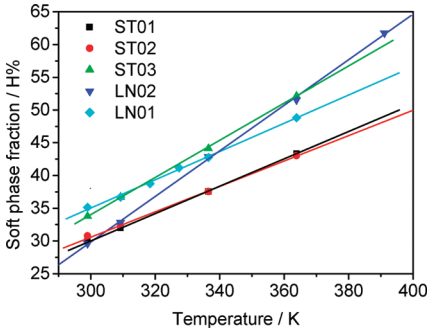

Figure 6. Soft phase fraction f_s in SBS's determined by MSE-refocused FID measurements.

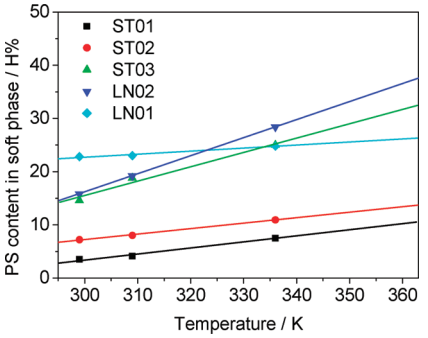

Figure 8. Polystyrene content in the soft phase from ^{1}H MAS NMR spectra as a function of temperature.

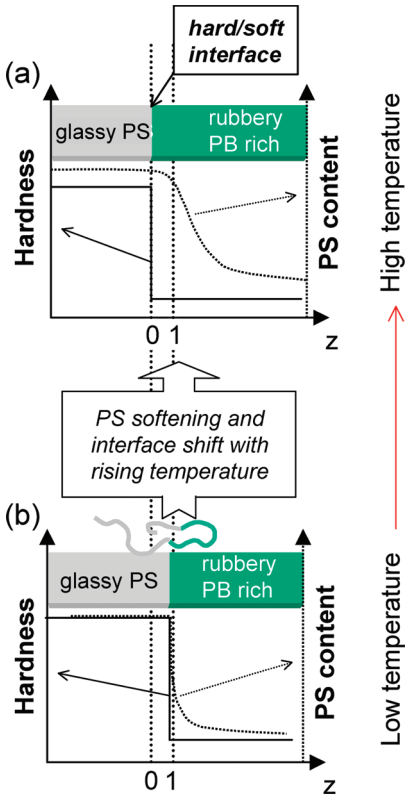

Figure 7. Scheme for the distinction between interfacial mobility and composition gradient in a glassy/rubbery system. The stepped hard/soft interface (solid line) is determined by the low-field solid-state NMR methods, and the information on the broad gradient compositional interface (dotted line) arises from high-resolution MAS experiments. With rising temperature, a part of the PS at the interface softens and integrates into the soft phase (→ "PS softening"), resulting in the broadened compositional gradient interface at higher temperatures as evidenced by the DQ-filtered MAS spin diffusion experiment. The hard/soft interface locations 1 and 0 at low and high temperatures, respectively, and the interface shift from soft to hard is also directly inferred from the NMR data.

3.2.1. Low-Field NMR: SBS Soft Phase Fraction as a Function of Temperature. The central piece of quantitative information from low-field NMR is the soft phase fraction of the SBS samples, as here determined between 299 and 400 K. From the point of view of solid-state NMR, at a temperature as high as 400 K, PS is still in the glassy state, since the segmental reorientations are still slower than the ~100 kHz needed for substantial averaging of dipolar interactions. The temperature dependence of the soft phase fraction of the different SBS's is shown in Figure 6.

In all SBS samples, the soft phase fraction increases with increasing temperatures. One can see that different amounts of hard phase soften upon heating, which is found to be dependent on the molecular parameters of the individual SBS's. As will be discussed in section 3.2.2, we know that the determined softened part mainly consists of PS. We therefore call the effect seen in Figure 6 "PS softening". In this context, it is again to be noticed that PB immobilization (probably at the interface) takes place to a rather minor extent only at lower temperature, i.e., between 299 and 336 K. This directly follows from our ^{1}H-based composition determinations described above and in ref 21 and from the data in Figure 3. The term "PS softening" is to emphasize that the softening is mainly due to PS and less due to the little amount of immobilized PB found at rather low temperatures and becomes mobile with the softening process. It should also be stressed again that the approach used here and explained in the experimental part (see Figure 2d) as well as in ref 21 proves a rather a sharp hard/soft interface, with only small contributions from somewhat mobilized interfacial PS, which can still be considered as part of the hard phase from the dynamic point of view.

As the temperature rises, the glassy/rubbery interface must therefore shift into the hard phase. Note that at any given temperature used in this study there is no indication of a substantial dynamic interphase (with an apparent T_2 in the range of 50−300 μs), i.e., a region with an in-between mobility. Yet, the failure to observe a distinctly different mobility gradient does not mean that there is no compositional gradient interphase. Figure 7 represents a schematic explanation of the sharp hard/soft interface defined by the solid-state NMR method and the compositional gradient interface. The issue of the compositional gradient will be treated in the following section. As will be seen, "PS softening" occurs at the interface and leads to an increased PS/PB composition gradient on the *mobile* phase side. Generally, the degree of "PS softening" is mirrored in the slopes in Figures 6 and 8, which could be used as a characteristic of the compositional interface gradient especially at elevated temperatures according to the following order: LN02 > ST03 > ST02 > ST01 > LN01.

The observed "PS softening" phenomenon can be explained by the enhanced motion of PS at the interface, where it is activated by the soft phase. Therefore, the chemical character of the soft phase and its compatibility with the hard phase must play an important role. Obviously, the degree of "PS softening" depends especially on the amount of PS comonomers incorporated into the mobile blocks in the SBS molecules, as is confirmed by the fact that the two Styrolux samples with a high statistical PS comonomer content in mobile blocks exhibit the steepest slope in Figure 6.

Yet, the "PS softening" phenomenon may also have a direct connection with the molecular weight and block length distributions. This means that SBS chains with a lower molecular weight and short PS blocks may soften first and move toward the soft phase. However, as the molecular weight and block lengths do not vary much in the investigated SBS samples, the slope difference between the samples seen in Figure 6 should be mainly due to the compositional difference in the mobile blocks. In any case, as long as the short PS blocks do not form separate phase-separated substructures and are thus not isolated from the long ones to a large extent, "PS softening", a reversible process, should occur at the interface. Vice versa, as the samples are cooled down, the softened PS along with the small amount of PB in some SBS returns to the interface. This interpretation is also corroborated by the results presented in the following section.

3.2.2. High-Field ^{1}H MAS NMR: Chemical Composition in the Soft Phase and at the Interface. High-field ^{1}H solid-state MAS NMR is able to detect chemical shifts especially in rubbery or other mobile and nonglassy materials. Here, we studied experimental temperatures varying from 299 to 363 K. Within this range, all SBS's have a distinct glassy/rubbery (hard/soft) mobility interface, in which the hard phase appears in the spectra as a broad hump which, in the narrow range of resolved signals, can be subtracted as part of the baseline (see Figure 2a−c). As explained in the experimental part, the chemical composition of the soft phase could be easily and quantitatively determined by integration of the aromatic and olefinic peaks, where the ratios of the 1,2-/1,4-polybutadiene contributions were always around 1/10.

Figure 8 shows the polybutadiene contents in the soft phase as a function of temperature. As can be seen, the PB content decreases, which means that the PS content increases with increasing temperature as a direct result of the "PS softening" described above. The largest change (steepest slope) is again found for the two samples ST03 and LN02, which have an intentionally high styrene comonomer content throughout the soft blocks (see Figure 1) and are consequently less well segregated (in a thermodynamic sense) from the PS hard phase (also cf. Figure 9). In contrast, ST01 and ST02 are synthesized without styrene comonomers in the soft blocks. Nevertheless, these samples still show significant "PS softening", but to a lesser extent. An interesting case is represented by the LN01 sample, which is originally designed as a gradient copolymer. It has the initially highest PS content in the soft phase, yet it shows the smallest change with temperature, indicating that there is less "PS softening". Apparently, the fixed gradient interphase in combination with the near-zero styrene content in the bulk of the soft phase is an *effective barrier for PS softening*. This phenomenon clearly deserves further investigation in the future. Moreover, we must also attend to the possibility of PB immobilization in the hard phase in this case.

Now we turn to the detailed interface composition, which was investigated with a DQ-filtered MAS spin diffusion experiment. In this experiment, the hard-phase magnetization was selected first. Then, with increasing spin diffusion time, well-resolved ^{1}H MAS spectra signals associated with the soft phase rise, from which the relative PS content can be calculated. In this way, we directly observe the composition in front of the interface in an interphase region that is defined by the increasingly broad Gaussian-type shape of the advancing magnetization profile (Figure 9). The spin diffusion time corresponds to the distance in the soft phase from the hard/soft interface and is strictly given by the width of a Gaussian-type profile. Here, two samples were chosen that exhibit

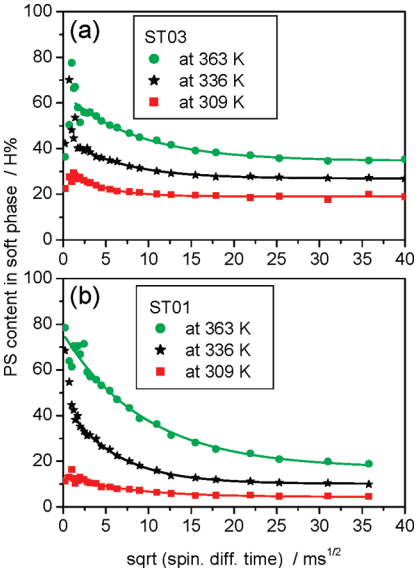

Figure 9. PS contents in the soft phase evaluated from the series of DQ-filtered ^{1}H MAS NMR spectra with increasing spin diffusion time. Two samples were chosen: that exhibit totally different behaviors (a) ST01 with weak and (b) ST03with strong "PS softening" (cf. Figure 8). The spin diffusion time is directly correlated with the increasing width of a half-Gaussian magnetization profile that has its maximum at the hard/soft interface and is therefore corresponding to the distance from the interface in the soft phase.

totally different "PS softening" behaviors according to Figure 8: ST03 with strong (Figure 9a) and ST01 with weak (Figure 9b) "PS softening".

The results in Figure 9, taken at 309, 336, and 363 K, clearly prove the different composition gradients in front of the interface. In both samples, the relative composition change as a function of spin diffusion time is weaker at lower temperatures, indicating a smaller composition gradient. In both cases, the initial PS content, detected at short spin diffusion time and thus close to the mobility interface, rises considerably upon raising the temperature. In ST01, the notable difference between the two temperatures is the large relative composition change. At low temperatures, the PS content in the mobile phase is very low and is mostly located at the interface (as it changes from an initial 15% to 5% on average during the spin diffusion process), while at high temperatures, the change is from 75% (much softened PS close to the interface) down to an average of ∼18%, which again is thus proven to be mostly close to the interface. The overall "contrast" for the PS interfacial softening is less for ST03, as it contains more styrene comonomers throughout the soft phase. However notably, the plateau characterizing the overall content is reached earlier at low temperatures, indicating that the additionally softened PS at high temperatures is located preferentially near the interface. As could be seen, there is still a certain amount of softened PS incorporated into the soft phase. This was already explained in the section above: as temperature is raised, the PS segments located at the interface are activated and "pulled" into the soft phase. Note that some SBS chains, preferably those with low molecular weight and shorter PS blocks, may move completely into the soft phase, at least partly resulting in the increased PS contents within the soft phase at a higher temperature (see Figure 9 at later spin diffusion time).

These observations fully support the scheme presented in Figure 7. Details on the data analysis using full simulation of the phenomenon are presented in a separate paper published recently.[33] In particular, the method is even sensitive to the

Table 2. Domain Sizes or Lamellar Thicknesses

		ST01	ST02	ST03	LN01	LN02
long period (nm)[a]	blend	36	42 17 (double)	≥39		29
	pure SBS	35	≥35 16 (double)	≥40	31	32
soft fraction at 299 K (vol %)		25.5	26.9	30.3	31.7	25.5
lamellar thickness of the hard phase (nm)[b]		26	≥25.5	≥28	21	24
lamellar thickness of the soft phase (nm)[b]		9	≥9.5	≥12	10	8
lamellar thickness of the soft phase (nm)[c]		13	12	14	11	11

[a] Determined with SAXS at room temperature, i.e., at about 299 K. The values are comparable with TEM/AFM micrographs. [b] Determined from the long period from SAXS and the soft phase fraction at 299 K from MSE experiments at low field. [c] Determined at 299 K by spin diffusion measurements at low field.

shape of the composition gradient, so that the experiment can be used to test theories of phase separation in block copolymers.

The sharp compositional interface gradient at lower temperature, i.e., 299 and 309 K, found in this study is in accord with a previous work[12] using ^{2}H NMR of poly (styrene-*block*-isoprene) labeled selectively at the block boundary, in which the authors deduced that the soft-component concentration should be negligibly small in the hard phase and that there is a dynamic interphase region of about 0.5 nm width at 300 K of a S−I block copolymer with a molecular weight M_w of 20 kDa (it seems that the higher the M_w value, the narrower the interphase region). Half a nanometer is negligibly narrow in comparison to the long period of about 40 nm in our SBS's of around 100 kDa. It should be noted that the compositional interphase region observed in our systems, where it spans a significant fraction of the soft phase, is generally much larger at higher temperatures. We should mention that the DQ-filtered ^{1}H MAS spin diffusion NMR results reflect the absolute size scale of the compositional interphase. Preliminary simulations are reported in ref 33, and future work will be devoted to establishing simple relationships between the spin diffusion time-dependent results and the true concentration profile.

Compared to the SAXS method[9] mentioned in section 3.1 to detect interphase width in phase-separated block copolymers, where strictly periodic morphologies and model assumptions are required, which cannot be met in extruded samples, the NMR methods used in this study showed the great advantage in investigation of compositional gradients at the interface of more polydisperse, industrially relevant samples.

3.2.3. Low-Field NMR: Soft-Phase T_2 Values and Relationship with the Chemical Composition. The T_2 relaxation time delivers information on the mobility of molecular chains or segments. This is quite simple if a sample is homogeneous without dimensional restriction involving tethers to an interface or to a hard (or glassy) phase. In block copolymers, the PB-rich soft phase is confined on a nanometer scale by a surrounding PS hard phase. In its simplest global interpretation, T_2 should primarily depend on the overall time scale of molecular mobility (that mainly changes with chemical composition, influencing the local T_g, and temperature) as well as the residual couplings within the nonisotropically mobile chains that are tethered at both ends to the rigid PS block.[26]

The latter quantity primarily depends on the chain length between the tethered ends in close analogy with the phenomenology observed in cross-linked elastomers[27,28] as well as on the interface hardness, which may be changed by "PS softening" upon raising the temperature. In case of the SBS samples used in this study, the soft phase domain sizes are all about the same as is seen in Table 2 (see Section 3.2.4). Therefore, the dimensional restrictions should not vary much, but the chemical composition and the interface hardness become the dominating factors influencing the T_2 value, which we studied at different temperatures.

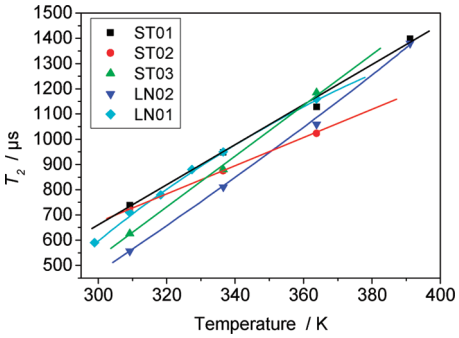

Figure 10. T_2 relaxation times in the soft phase of the SBS's vs temperature. The lines are only guides to the eye.

Figure 10 sums up the temperature dependence of T_2 in the soft phase of the SBS's. It is to be expected that T_2 values of rubbery polymers increase with increasing temperatures. Generally, with the same mesoscopic spatial restrictions (block size) and same interface hardness, T_2 at a certain temperature should mostly depend on the styrene comonomer incorporation into the soft phase. However, we suppose that this is only true (and is indeed observed) if the temperature remains at the lower end of the interval studied (299 K). As the temperature rises, the T_2 values in samples LN02 and ST03 increase more rapidly than in other samples and become even higher as the temperature reaches ~400 K. This can be qualitatively explained in terms of the stronger "PS softening" effect in LN02 and ST03, where the interface becomes much "softer", which leads to an overall higher mobility and an increase in the T_2 values. It must, however, be kept in mind that the high-temperature T_2 values are more and more dominated by residual couplings as a result of the block-size-dependent restriction to the chain ends (network-like situation), which yields an upper limit ("T_2 plateau") when the chain sweeps out its whole conformational space, and that a comparison is then only feasible for samples with overall similar domain sizes.

These arguments and observations are corroborated by a recent study on residual dipolar couplings in differently cross-linked natural rubber,[29] where at low temperatures local mobility and packing dominate over the cross-links. In the present case, T_2 values, which are more influenced by 20 kHz-scale mobility rather than by geometric constraints, are most reliably measured at the lowest temperature of 299 K, which is just far enough above the glass transition of the soft

phase, yet low enough to avoid a dominating effect of residual couplings (related to morphology rather than composition) on T_2, and well below the onset of the broad glass transition of the hard phase.

In this context, we note that the observation of a singly exponential T_2 is somewhat unexpected, since (i) T_2 decays dominated by dephasing due to residual dipolar couplings are often closer to Gaussian or Weibullian (i.e., with an exponent lower than 2) functions and (ii) a superposition due to the heterogeneous nature of the interphase (composition gradient) and due to different microenvironments can be expected. We explain our finding with a cancellation of the two effects: superpositions of Gaussian- or Weibullian-shaped functions can indeed appear exponential, in particular when they are superposed with effects of molecular motion (true relaxation), that in a simple approximation lead to an additional, often dominant exponential decay factor. The latter is dependent on the time scale of segmental motion, and this in turn depends on the temperature offset above T_g, and this in turn depends on composition.

In order to establish simple and cost-efficient low-field NMR as a simple alternative to the high-field ^{1}H MAS NMR method to determine the butadiene content in the soft phase, we used the total butadiene contents calculated from solution NMR spectra (usually routinely available) and the soft phase fractions known from MSE experiments on the Minispec, under the *assumption* that all PB resides within the soft phase (for detailed arguments, we refer to the experimental part). The simple method, which requires no high-field solid-state NMR machine, is also rather time- and cost-efficient, and an in-depth explanation and details supporting the assumption were presented in the section 2.2 part "Determination of phase composition". For the following, we included an even larger number of SBS samples to improve the statistical relevance of our experimental results.

Comparing the simplified method to the ^{1}H MAS NMR method for butadiene contents determination in the soft phase, there is reasonable agreement for samples with T_2 exceeding 500 μs at the low temperature of 299 K (Figure 11a). For higher T_2 values, the "simple" approach (gray triangles) appears to fail, while T_2 is still observed to correlate well with the true soft-phase composition (red squares), determined by the more laborious high-field MAS NMR approach. This merely shows the limitations of the simple, indirect composition determination, which fails at lower temperatures due to the amount of PB that is immobilized in the hard phase. As detailed in section 2.2 and in part "Determination of phase composition", at temperatures above 336 K all SBSs used in this study proved to have hard phases free of PB, and the simple approach can be used to evaluate the chemical composition of the soft phase. For an interpretation of the T_2, this means that at lower temperature the overall mobility in the soft phase is completely dominated by composition and that effects due to constraints to the chain ends are weak.

Figure 11b shows results of attempted correlations using soft-phase compositions from the simple approach at 400 and 363 K (the former being obtained by extrapolating the temperature dependence of the soft fraction in Figure 6) and T_2 at 299 and 363 K, respectively (the 363 K pair is shown as inset). Again, note that from Figure 11a it is clear that T_2 scales well with composition only at 299 K, while the simple indirect method for composition determination is correct only above 336 K. At a first glance, the good correlation between the simple low-field accessible quantities taken at very different temperatures is surprising. We consider this correlation most interesting for high-throughput screening

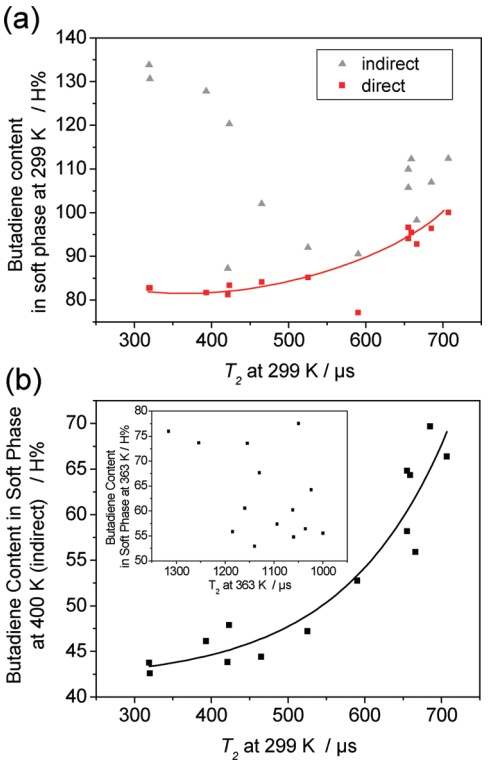

Figure 11. Correlations of T_2 and the comonomer content in the soft phase. (a) Soft-phase composition at 299 K (from direct and indirect methods) in relation to T_2 at 299 K. (b) Correlation of the comonomer content in the soft phase at 400 K (from indirect method) with T_2 at 299 K. The 14 data points are from different block copolymers with different molecular designs, similar to the ones shown in Figure 1. Inset: bad correlation for both quantities evaluated at 363 K.

applications. Essentially, the result indicates that soft-phase compositions at 299 and 400 K are directly correlated for all samples. As temperature increases, the interface softens and the chain dynamics speeds up, leading to complex changes in T_2, as mentioned above, and chemical composition ceases to be the only influencing factor, which explains the missing correlation at 363 K shown in the inset.

As to an interpretation, the good correlation suggests that the extent of PS softening at a higher temperature, which of course changes the PS content in the soft phase as compared to the lower temperature, can be concluded to be on average *proportional* to the PS contents of the soft phase at a lower temperature. This conclusion is rather interesting, in that it again proves the earlier conclusion that actual interfacial composition gradients, present in some of the samples, do not have much effect on the softening behavior—it is only the overall PB content of the soft phase that matters, suggesting an averaged thermodynamic driving force related to overall miscibility (segretation strength).

Note, however, that the correlation in Figure 11b may not be a general rule to be applied to other block copolymer systems. It may be only valid for the SBS block copolymers with similar soft phase sizes and lamellar morphology, which is true in our case, as will be shown in the following sections. The restricting and softening influence of the interface on the hard and soft phases, respectively, will be addressed in future work, where we will report on the application of multiple-quantum spectroscopy (also done on the Minispec), which offers the potential to reliably separate the effect of the actual time scale of chain dynamics and the effect of residual dipolar couplings induced by confinement on T_2.[29,30]

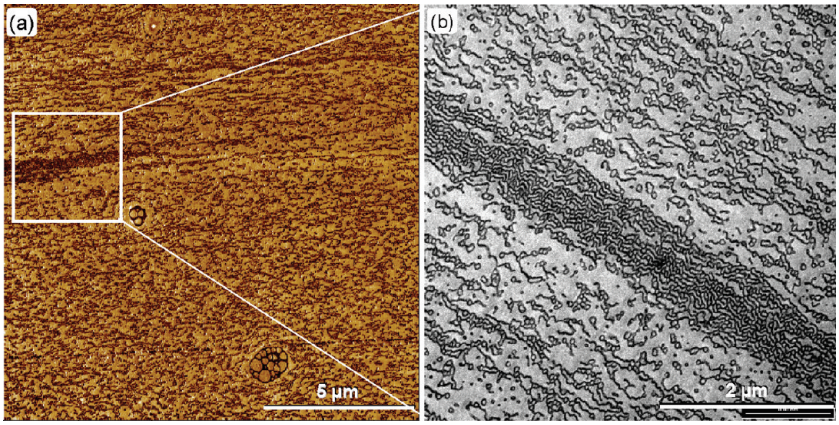

Figure 12. Comparison of an AFM phase image (left) and a TEM micrograph (right) of a ST03/GPPS 40/60 blend. In the AFM phase image, the polybutadiene-rich phase appears darker because it is softer than the PS phase. In TEM, the polybutadiene-rich phase appears darker because the double bonds are more stained with OsO_4.

3.2.4. Domain Sizes Determined by ^1H Spin Diffusion at Low Field, SAXS/MSE and TEM. ^1H spin diffusion readily yields the domain size especially for the soft phase as averaged value over a whole sample, as does SAXS, whereas TEM measures a localized area in the micrometer range. Staining effects and effects of over/lower focusing of the electron beam limit the evaluation of absolute lamellar thickness in TEM micrographs. For the calculation of domain sizes with the spin diffusion method, calibrations and model assumptions concerning the morphology (lamellae vs cylinders) are needed.[20,21] We assume lamellar morphology in all cases, which is at least true for most SBS/PS blends, as seen in the TEM micrographs (see Figures 13 and 14). As mentioned in section 3.1, the difference in the long periods is quite small when blends and the respective pure block copolymers are compared (Figure 5), which means that the block copolymers remain clustered rather than being homogeneously dispersed by PS (see TEM micrographs). The ordering of the block copolymers is even slightly enhanced in blends, as could be confirmed by TEM and SAXS diagrams. This means the SBS′s in blends are more lamella-like than in pure SBS, partially because the blends are extruded plates and the pure SBS are granules. Therefore, we chose the 40/60 SBS/PS blends to evaluate lamellar thicknesses, using the spin diffusion procedure described in the experimental part. Because no strictly periodic structure is needed, the spin diffusion method offers advantages for lamellar thickness evaluation as compared to SAXS.

Also, by combining the soft phase fraction determined by MSE measurements and the long period determined by SAXS, the lamellar thickness both of the soft PB-rich and the hard PS in the block polymers can be estimated in an alternative way. Blends could not be treated in this way because, as mentioned above, the SBS lamella-like morphologies are not homogeneously dispersed throughout the blend samples. Yet, we suppose that the lamellar thicknesses of the PB-rich phases in SBS remain the same as in blends; a detailed check would certainly be worthwhile. According to SAXS, at least the (apparent) long periods are the same both in pure SBS and SBS/PS blends.

Comparing the results from SAXS/MSE, TEM, and spin diffusion (Table 2), we find that in particular for PB-rich soft phases (ST01 and ST02) spin diffusion measurements yield considerably larger values than those calculated from the SAXS long period and the hard/soft volume ratio. This may at a first glance be due to the fact that a well-ordered lamellar structure is assumed in the evaluations and the model

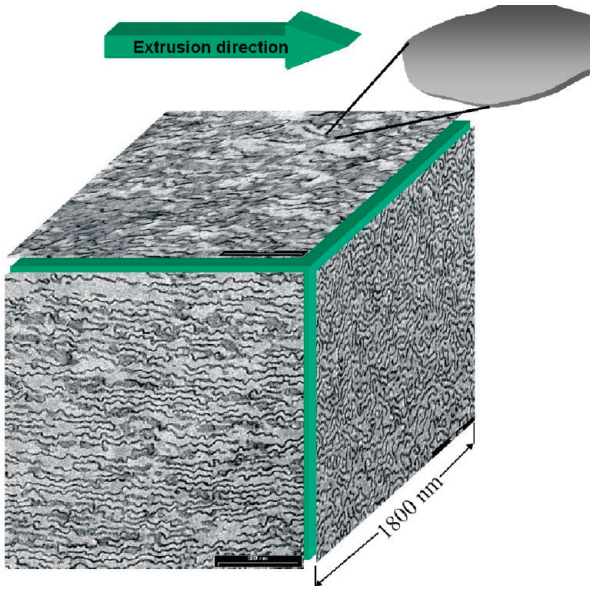

Figure 13. 3D-TEM illustration of the ST01/GPPS 40/60 blend morphology. Images from three orthogonal directions were taken from the same area at a distance of about 150 μm from the surface of a 1 mm thick extruded sheet. Sections were taken from three directions separately, all at this depth. The images were projected on a cube according to their direction. The lamellae are orientated along the extrusion direction; i.e., they are parallel to the surface and elongated along the extrusion direction, indicated by an enlarged schematic.

calculations for the data obtained by all methods and that different systematic deviations arise when this assumption is not fully met. A second point is that the systems are, after all, rather polydisperse in their morphology, and the different methods provide different types of averages. Third, spin diffusion depends on mobility contrast, while SAXS is sensitive to electron density, whereby not only mobility (above or below T_g) but also composition plays a role. Finally, the T_2-based calibration procedure for the spin diffusion data should probably be revised in the light of the above-mentioned effects of the compositional heterogeneity in the interface region, which is beyond the scope of this work.[21] It should, however, be emphasized that spin diffusion, by nature of the process, emphasizes the shortest distances in the system and that it has the intrinsic property of differentiating between hard and soft domains. It might therefore carry the highest potential for detecting the phase

separation length scale that could carry the most meaningful correlation with mechanical properties.

3.3. Morphologies in Extruded SBS/PS Blends and Their Mechanical Properties. Both TEM and AFM are able to visualize the morphology of block copolymers and blends. For our investigation it was necessary to visualize the bulk morphology. For TEM, microtomed sections were investigated. On the other hand, AFM investigations performed on the surface of bulk samples or films can produce misleading results with regard to bulk morphologies because the surface morphology can greatly differ from the one in the bulk.[24] Therefore, it is important to study the bulk morphology with AFM by using microtomed samples. For comparison, Figure 12 shows the morphology of a 40/60 ST03/GPPS blend visualized both by TEM and AFM. For TEM, staining of the samples with OsO_4 was needed. The micrographs taken with the respective techniques were practically identical. In both micrographs, brighter areas corresponded to glassy PS-rich material, which formed the matrix, and darker areas corresponded to PB-rich lamellae and lamellae-like structures. On the one hand, with AFM an overlook image with a much larger scale could be easily obtained because no ultrathin sections with homogeneous thickness were needed, while on the other hand, with TEM a much better contrast and a more detailed morphology could be resolved without the noise of cutting traces and cantilever artifacts. This was discussed in detail in our previous paper.[25] As the two methods can give practically identical information, we mainly discuss the TEM micrographs in the following.

To study the blend morphology, extruded sheets of about 1 mm thickness were investigated. Depending on the extruding direction and the location depth from the sample surface, the blend morphology varies considerably within the sample. The influence of both parameters on the morphology was studied. It was found that depth has a significant influence on the morphology. At the depth very close to the surface, i.e., within several micrometers from surface, an enrichment of PS and a more inhomogeneous morphology was found. To investigate the effect of orientation, ultrathin sections from three orthogonal directions were investigated by TEM. These sections were taken from an area at a depth of about 150 μm from the surface of the sheets. Figure 13 shows the projection of images obtained from sections taken from the three directions. The block morphology is clearly oriented along the extrusion direction of the ST01/GPPS 40/60 blend. The sample shows a lamellar morphology. The lamellae appear extended along the extrusion direction and are clearly curved. On the top of the cube mainly flat-on lamellae are visible, whereas the front face of the cube shows the lamellae edge-on. As shown schematically, the lamellae are oriented parallel to the surface and are elongated along the extrusion direction. Note that the samples are in the "as-is" state; i.e., they originated from extrusion processing at 170 °C and subsequent cooling and annealing at 70 °C.

For consistency, the following morphologies were all taken at a location 150 μm below the sample surface and, second, a cross-section perpendicular to the extrusion direction, i.e., the right face of the cube in Figure 13. Figure 14 shows the typical morphologies of the 40/60 wt % SBS/PS blends comprising block copolymers with a different molecular architecture (see Figure 1). Although the total butadiene/styrene contents in the block copolymers are about the same (Table 1), quite different and characteristic blend morphologies could be identified for the respective SBS's. The morphologies of the different blends can be described as follows: Within the PS matrix, different kinds of lamellae or a lamellar-like morphology of polybutadiene-rich phases are observed. The ST01/GPPS blend shows disordered, highly curved lamellae (Figure 15a). In the ST03/GPPS blend (Figure 14b), the polybutadiene-rich phase forms a morphology resembling a continuous network dispersed in a PS matrix. The sample shows also a strong tendency to form tubelike polybutadiene-rich phases (perpendicular to the image) which are connected mostly by lamellae in-between (see Figure 15 for a scheme of this morphology). The two blends LN01/GPPS and LN02/GPPS (Figure 14c,d) show well-defined and more or less ordered lamellar morphologies with extended lamellar stacks. The difference between the two samples is that the blend LN02/GPPS forms longer continuous lamellae than the blend LN01/GPPS. Short and long lamellae are marked red in the respective pictures. The sample ST02/GPPS (Figure 14e) has a very special double lamellar structure. This morphology was also reported in earlier publications for SBSs with a similar molecular architecture[2,7] and may be the result of an intermolecular phase separation between long and short PS blocks in the starlike block copolymers. Particularly the styrene core of ST02 appears to be the driving force for different PS domains. This morphology becomes more expressed when small amounts of low molecular weight PS are added to the blend. Because low molecular weight PS can be incorporated within shorter PS blocks, this makes the double lamellae appear clearer (Figure 14f).

The tendency of double lamellar formation (PS hard phase sandwiched between soft-phase lamellae) was also verified by SAXS (Figure 5b,c).

One of the important results of this study is that the SBS's with more styrene comonomer incorporated into the mobile blocks of the block copolymer molecules, which thus exhibit stronger "PS softening" and compositional interface gradients at elevated temperatures, like ST03 and LN02, can form a long and more continuous lamellar morphology in the SBS/PS blends, which could favor the impact modification of blends. As shown in section 3.2.3, the styrene contents of the soft phase, even near the PS glass transition, are well reflected in the T_2 value measured at 299 K (because the PS softening at higher temperatures is stipulated to be proportional to the PS contents at 299 K). Ultimately, it is the composition in the phase-separated melt state, at temperature above T_g, of PS, that is a key factor in the morphology formation process, and the morphologies in turn are important for the different mechanical properties.

Therefore, we attempted a correlation of the mechanical properties of the 50/50 wt % blends, i.e., the elongation at break (strain at break, being related to the ductility) and T_2 at 299 K, as is shown in Figure 16. Note again that the T_2 is the most easily determined quantity, requiring only a simple low-field NMR measurement performed on an arbitrarily shaped sample in around 10 min or less. We assume that the rather large scatter in the data is most probably due to the difficult reproducibility of the strain at break measurements, as is indicated by the 20−30% standard deviation, as compared to 2% for T_2 measurements. Obviously, the good ductility, meaning improved impact property, is to some extent attributable to the continually dispersed SBS morphologies in the blends, which is in turn correlated with the compositional interface gradient and polystyrene incorporation in the PB-rich phase. In summary, we can conclude that the continuous SBS morphology in SBS/PS blends, which favors the ductility, could be achieved by simply increasing the PS content in the mobile blocks of the SBS molecule chains. Apart from that, a double lamellae morphology appearing (preferably) in asymmetric star-shaped SBS block

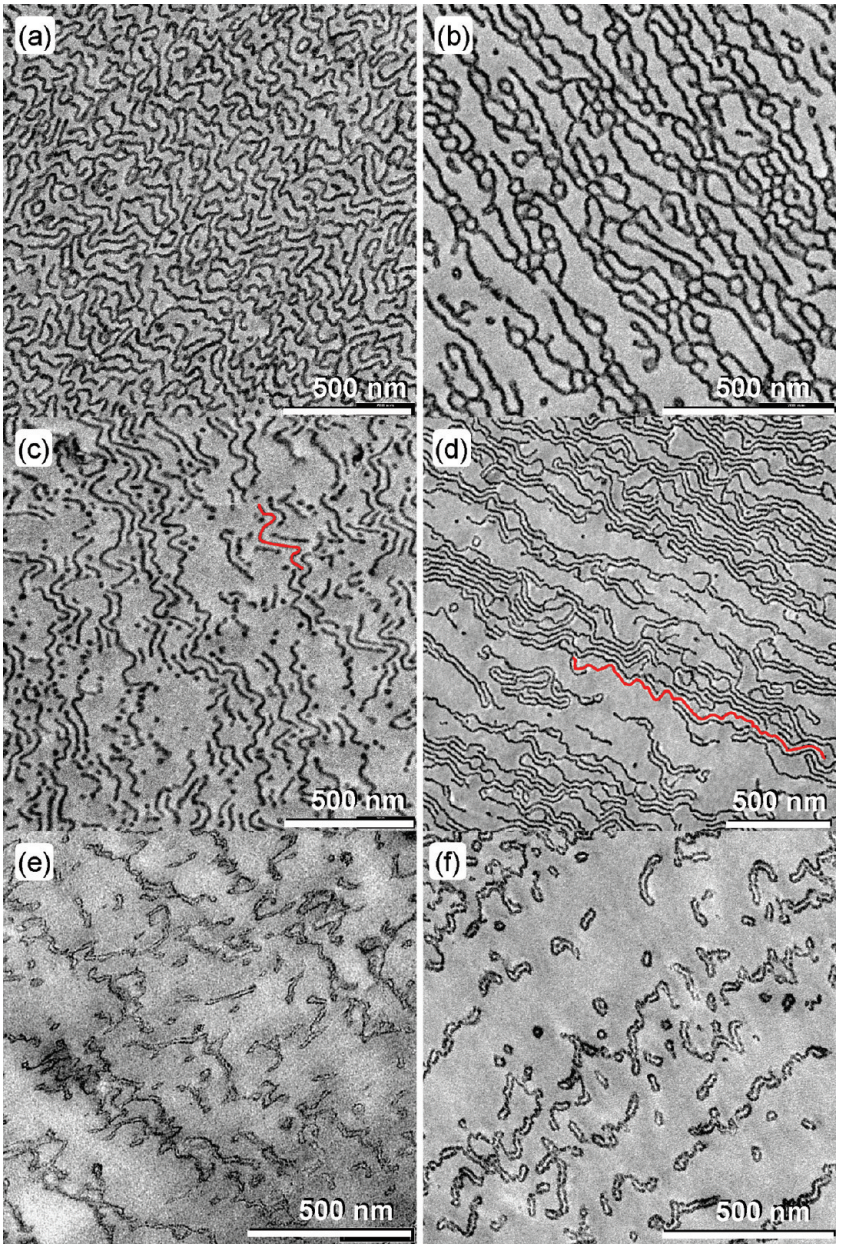

Figure 14. TEM micrographs. Morphologies of the 40/60 SBS/GPPS blends. The images are all taken from the plane perpendicular to the extrusion direction. (a) ST01/GPPS blend; (b) ST03/GPPS; (c) LN01/GPPS; (d) LN02/GPPS; (e) ST02/GPPS; (f) ST02/GPPS with small amount of low molecular weight PS. Long and short lamellae are marked with red lines in the blends LN01/GPPS and LN02/GPPS.

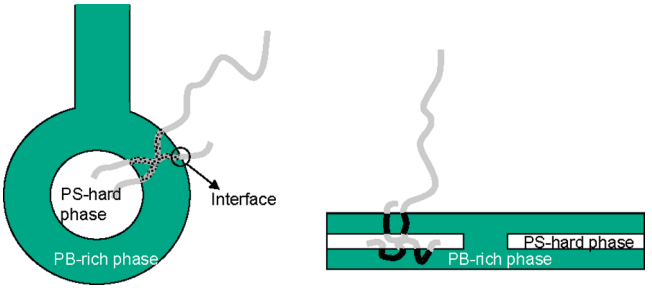

Figure 15. Two special SBS molecular self-organization modes other than ordinary lamellar morphology: left is assigned to ST03 and right to ST02 with double lamellar morphology.

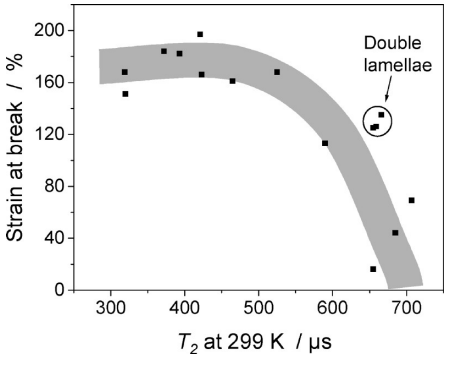

Figure 16. Correlation of the tensile ductility (strain at break ε_B) with T_2 of the 40/60 wt SBS/PS blends.

copolymers can obviously, to some extent, also influence the ductility of SBS/PS blends. Note that the data points within the circle in Figure 16, which deviate significantly from the general trend, are from block copolymers with double lamellae.

Again, we must emphasize that the T_2 correlation shown in this study is not necessarily generally applicable to other block copolymer systems. The correlation in Figure 16 is valid because the T_2 values at room temperature are directly correlated to the soft-phase composition, and these composition differences persist even at high temperatures, where it could be extrapolated into the PS melt state, in which the morphology forms. For other systems, T_2 at lower temperature will certainly also reflect the soft-phase composition, yet whether this is predictive for the composition at higher temperature depends on parameters such as molecular weight, overall chemical composition, and comonomer types, which should be carefully considered to obtain specific correlations.

3.4. Useful Information and Low Field NMR Methods Applicable for High Output Polymer Screening. For "combinatorial materials research" (CMR) and high output polymer screening (HOPS), analytical tools for rapid characterization are required, preferably as online measurement implemented into fully automated screening workstations. The high output oriented screening combines automated reactors and processing with rapid online polymer characterization in order to accumulate and process the information required to develop new polymerization processes, catalysts, initiator systems, and compounding. An important issue of HOPS is to improve the exploitation of high information density per experiment.[14] When this information is combined with modeling and simulation tools, it is possible to derive "fingerprints" correlating spectroscopic properties with materials properties and processing. This correlation is very useful for technology transfer into production and the development of online quality control systems. For the development of many multiphase and multicomponent materials similar to those under investigation in this study, the costly and time-consuming TEM/AFM and SAXS as well as high-field solid-state NMR are until now the almost only way to obtain direct morphological information and molecular parameters in the solid state. These methods require skilled employees and intensive manual intervention, and they severely slow down the speed of automated synthesis workstations and high output oriented screening systems. Moreover, their high costs limit their applications in online and off-line quality control systems for the industrial production of such materials.

In this study, rapid and cost-efficient low-field pulsed NMR methods were introduced, and meaningful correlations of their results with those of TEM and high-field NMR were established. Although often having been developed for high-field NMR, many even complicated pulse programs such as the MSE or the combined MSE−spin diffusion experiment can easily be implemented on a low-field NMR such as Minispec.[21] In spite of its low resolution, low-field NMR can deliver results that are comparable to those obtained at high field, when the observables are dominated by effects of dipolar couplings, which is the case for all the effects studied here. The actual experiments on a low-field NMR as well as the data processing can easily be automated and are therefore suitable for online screening.

In summary, low-field NMR can deliver the following characteristics for the study of SBS systems:

(1) "PS softening" effects can be detected by temperature-dependent hard/soft ratios, evaluated from MSE-refocused FID's.
(2) This enables a simplified method to determine the chemical composition in the soft phase from the hard/soft ratio and the total chemical composition known from solution-state NMR, which could be easily calculated as long as there is no butadiene residing in the hard phase, which is the case at temperatures higher than about 336 K in this study.
(3) Domain size measurements are possible with spin diffusion experiments.
(4) T_2 values measured with Hahn-echo experiments at room temperature (299 K) can be correlated to the chemical composition of mobile blocks in SBS's, and thus to the interface gradients even at elevated temperatures, which determine the tensile ductility of SBS/PS blends. The correlation is for this class of copolymers explained by the fact that the extent of PS softening and presumably the composition of the phase-separated melt above T_g of PS are apparently proportional to the PS comonomer contents at lower temperature, indicating that overall miscibility rather than comonomer sequence close to the interface (such as gradient linkages) are most important.

Not only the experiments used in this study but also other new advanced pulsed solid-state NMR methods, which have been developed in recent years, could provide information on the structure and dynamics of either heterogeneous or homogeneous polymers and elastomers.[31] Even advanced multiple-quantum experiments can easily be implemented in low field NMR experiments without any sacrifice in data quality.[32] The latter class of experiments was applied to the presently investigated samples in order to elucidate details of the T_2 process, and these results will be reported elsewhere.

4. Conclusions

Different degrees of "PS softening" were found in the studied SBS samples as the temperature was raised from room temperature up to the PS glass transition temperature. This holds in general, and the phenomenon is mainly dependent on the PS comonomer contents of the soft phase, as defined by the synthesis. Although there is actually a small amount of PB segments entrapped in the hard phase at lower temperatures (with some dependence on the comonomer content in the mobile blocks of the SBS's), this PB moves into the soft phase along with the "PS softening". The term "PS softening" is meant to emphasize that the softening process observed in this study is mainly due to PS itself which moves into (or becomes part of) the soft phase and less due to the small PB amount immobilized in the hard phase, since at temperatures above 336 K, PS softening goes on, while separate quantitative experiments prove the absence of PB in the hard phase (see Figure 3b). An open question is whether the immobilized PB at lower temperatures is (1) fully entrapped, either molecularly mixed or forming some "mosaic"-like substructures in the hard domains, or (2) retains some small-amplitude mobility at the interface. Certainly, option 1 cannot be true if PS blocks are synthesized without butadiene incorporation within the blocks, which is the case for the SBS samples in this study. As for option 2, the failure to detect a substantial rigid/mobile interface mobility gradient with the low field ^{1}H NMR methods at any temperature suggests at least a negligibly small volume fraction of such "dynamic interphases". The rather sharp hard/soft (or glassy/rubbery) interface moves from the soft into the hard phase, explaining the PS softening phenomenon.

Nonetheless, *compositional* gradients at the interface, both in the soft phase and at the sharp hard/soft interface, could be directly observed by hard-phase selected spin diffusion experiments resolved by high field ^{1}H MAS NMR spectra. We found that at around room temperature all the studied SBS's showed relatively sharp compositional gradients, but as temperature increases up to 363 K, the interface gradient region becomes broadened (and the gradient is thus shallower). Along with the

trend of different extents of "PS softening" in the different samples, the spatially resolved compositions also reflect that PS close to the interface softens and becomes partially mixed into the soft phase. We cannot exclude that whole SBS molecules, preferably with lower molecular weight and shorter PS blocks, can entirely move into the soft phase. But during the softening process, most of the softened PS remains at the interface, forming a compositional gradient. The whole process must be fully reversible within the time scale of the practical extrusion process and appears to be at least metastable, though not necessarily in thermodynamic equilibrium. True equilibrium arguments apply only for the order−disorder transition temperature, which is conventionally discussed in relation to scattering phenomena of block copolymers.

As the molecular weight, distribution, and block lengths in the studied SBS samples do not vary much, we concluded that the degree of compositional broadening at the interface depends mainly on the amount of styrene statistically copolymerized into the mobile blocks. For example, the high styrene content in the mobile blocks of the samples ST03 and LN02 proved to have a strongly broadened interface gradient. However, this could not be found in the sample LN01, where gradient linkages between the blocks in the SBS molecules were specifically synthesized. We can therefore conclude that the broadened gradient interface is mainly due to an improved compatibility between the PS phase and the PB-rich phase in SBS's or PS/SBS blends. A gradient block linkage in the block copolymer molecules does not improve the compatibility—it in fact stabilizes the interface and suppresses PS softening. With the initial PS content in the soft phase as the major control variable, we assume that the interfacial composition gradients that develop upon heating can be extrapolated into the melt state, where morphologies are primarily formed, with substantial influence on the mechanical properties. As for the influence of SBS molecular shape on morphology formation, it was found that the star block copolymers, particularly those with short PS core blocks, preferentially give rise to a typical double lamellar morphology, which was detected by SAXS and TEM. The double lamellae was found to some extent to positively affect the blends compact mechanical property but have no specific influence on PS softening.

Hereupon we established the correlation between "PS softening", interface gradient, morphology formation in SBS/PS blends and their resulting mechanical properties with industrially relevant samples, emphasizing the utility of NMR techniques. Last but not least, low-field NMR methods have been proven to be potentially useful tools for HOPS (high-output polymer screening) developments, i.e., for online monitoring and quality control in pilot plants and the industrial production of such materials. The most decisive advantages of low field solid-state NMR are that it is cost-efficient, robust, rapid, and easy to use. Its results are correlative to those of the advanced high field methods. Besides that, temperature programs and data analysis routines can be easily automated for screening applications.

Acknowledgment. This study has been financially supported by the Bundesministerium für Bildung und Forschung (BMBF project 03C0354A), the Deutsche Forschungsgemeinschaft (SFBs 418 and 428), and Fonds der Chemischen Industrie.

References and Notes

(1) Phillips Petroleum US 3078254, 1963, and BASF US 6593430, 2003.
(2) (a) Holden, G.; Legge, N. R. In *Thermoplastic Elastomers*, 2nd ed.; Holden, G., Legge, N. R., Quirk, R. P., Schroeder, H. E., Eds.; Hanser: Munich, Germany, 1996. (b) Knoll, K. In Polystyrol. *Kunststoff Handbuch IV*; Becker, G. W., Braun, D., Eds.; Carl Hanser Verlag: München, Wien, 1996.
(3) Knoll, K.; Niessner, N. *ACS Symp. Ser.* **1996**, *696*, 112.
(4) Fahrbach, G.; Gerberding, K.; Mittnacht, H.; Seiler, E.; Stein, D. DE 2610068, **1977**.
(5) Michler, G. H.; Adhikari, R.; Lebek, W.; Goerlitz, S.; Weidisch, R.; Knoll, K. *J. Appl. Polym. Sci.* **2002**, *85*, 683.
(6) Adhikari, R.; Michler, G. H.; Huy, T. A.; Ivankova, E.; Godehardt, R.; Lebek, W.; Knoll, K. *Macromol. Chem. Phys.* **2003**, *204*, 488.
(7) Adhikari, R.; Huy, T. A.; Buschnakowski, M.; Michler, G. H.; Knoll, K. *Polymer* **2004**, *45*, 241.
(8) Adhikari, R.; Huy, T. A.; Buschnakowski, M.; Michler, G. H.; Knoll, K. *New J. Phys.* **2004**, *6*, 28.
(9) Hashimoto, T.; Fujimura, M.; Kawai, H. *Macromolecules* **1980**, *13*, 1660.
(10) Hale, A.; Bair, H. E. *Thermal Characterization of Polymeric Materials*, 2nd ed.; Academic: San Diego, 1997; p 747.
(11) Spontak, R. J.; Williams, M. C.; Agard, D. A. *Macromolecules* **1988**, *21*, 1377.
(12) Stöppelmann, G.; Gronski, W.; Blumen, A. *Polymer* **1990**, *31*, 1838.
(13) Olvera de la Cruz, M.; Sanchez, I. C. *Macromolecules* **1986**, *19*, 2501.
(14) Tuchbreiter, A.; Marquardt, J.; Kappler, B.; Honerkamp, J.; Kristen, M.; Mülhaupt, R. *Macromol. Rapid Commun.* **2003**, *24*, 1.
(15) Clauss, J.; Schmidt-Rohr, K.; Spiess, H. W. *Acta Polym.* **1993**, *44*, 1.
(16) (a) Litvinov, V. M.; Penning, J. P. *Macromol. Chem. Phys.* **2004**, *205*, 1721. (b) Litvinov, V. M.; Soliman, M. *Polymer* **2005**, *46*, 3077.
(17) (a) Rhim, W.-K.; Pines, A.; Wauch, J. S. *Phys. Rev. B* **1971**, *3*, 684. (b) Matsui, S. *Chem. Phys. Lett.* **1991**, *179*, 187.
(18) Maus, A.; Hertlein, C.; Saalwächter, K. *Macromol. Chem. Phys.* **2006**, *207*, 1159.
(19) Goldman, M.; Shen, L. *Phys. Rev.* **1966**, *144*, 321–331.
(20) Mellinger, F.; Wilhelm, M.; Spiess, H. W. *Macromolecules* **1999**, *32*, 4686.
(21) Mauri, M.; Thomann, Y.; Schneider, H.; Saalwächter, K. *Solid State Nucl. Magn. Reson.* **2008**, *34*, 125–141.
(22) Egger, N.; Schmidt-Rohr, K.; Blümich, B.; Domke, W.-D.; Stapp, B. *J. Appl. Polym. Sci.* **1992**, *44*, 289.
(23) Strobl, G. R. *Acta Crystallogr.* **1970**, *A26*, 367.
(24) Thomann, Y.; Thomann, R.; Bar, G.; Ganter, M.; Machutta, B.; Mülhaupt, R. *J. Microsc.* **1999**, *195*, 161.
(25) Ott, H.; Abetz, V.; Altstadt, V.; Thomann, Y.; Pfau, A. *J. Microsc.* **2002**, *205*, 106.
(26) Dollase, T.; Graf, R.; Heuer, A.; W. Spiess, H. *Macromolecules* **2001**, *34*, 298.
(27) Cohen-Addad, J. P. *Prog. NMR Spectrosc.* **1993**, *25*, 1.
(28) Saalwächter, K.; Herrero, B.; López-Manchado, M. A. *Macromolecules* **2005**, *38*, 9650.
(29) Saalwächter, K.; Heuer, A. *Macromolecules* **2006**, *39*, 3291.
(30) Saalwächter, K.; Ziegler, P.; Spyckerelle, O.; Haidar, B.; Vidal, A.; Sommer, J.-U. *J. Chem. Phys.* **2003**, *119*, 3468.
(31) (a) Schmidt-Rohr, K.; Spiess, H. W. *Multidimensional Solid-State NMR and Polymers*; Academic Press: London, 1994. (b) Litvinov, V. M., De, P. P., Eds. *Spectroscopy of Rubbers and Rubbery Materials*; Ropra Technology Ltd.: Shawbury, 2002.
(32) Saalwächter, K. *J. Am. Chem. Soc.* **2003**, *125*, 14684.
(33) Saalwächter, K.; Thomann, Y.; Hasenhindl, A.; Schneider, H. *Macromolecules* **2008**, *41*, 9187.